



Enzyme-like biomimetic oral-agent enabling modulating gut microbiota and restoring redox homeostasis to treat inflammatory bowel disease

Zhangpeng Shi^{a,b}, Xiaohong Li^b, Jufeng Chen^b, Zideng Dai^b, Yefei Zhu^a, Tan Wu^{a,c}, Qing Liu^b, Huanlong Qin^{a,*}, Yang Zhang^{a,c,**}, Hangrong Chen^{a,b,***}

^a Nanotechnology and Intestinal Microecology Research Center, Shanghai Tenth People's Hospital, School of Medicine, Tongji University, Shanghai, 200072, PR China

^b State Key Laboratory of High Performance Ceramics and Superfine Microstructure, Shanghai Institute of Ceramics, Chinese Academy of Sciences, Shanghai, 200050, PR China

^c School of Pharmacy, Anhui Medical University, Hefei, 230032, PR China

ARTICLE INFO

Keywords:

Inflammatory bowel disease
Biomimetic oral-agent
Gut microbiota modulation
ROS-Inflammation
Yeast cellular wall

ABSTRACT

Reactive oxygen species (ROS), immune dysregulation-induced inflammatory outbreaks and microbial imbalance play critical roles in the development of inflammatory bowel disease (IBD). Herein, a novel enzyme-like biomimetic oral-agent ZnPBA@YCW has been developed, using yeast cell wall (YCW) as the outer shell and zinc-doped Prussian blue analogue (ZnPBA) nanozyme inside. When orally administered, the ZnPBA@YCW is able to adhere to *Escherichia coli* occupying the ecological niche in IBD and subsequently release the ZnPBA nanozyme for removal of *E. coli*, meanwhile exhibiting improved intestinal epithelial barrier repair. Moreover, it is found that the ZnPBA nanozyme exhibits remarkable capability in restoring redox homeostasis by scavenging ROS and inhibiting NF- κ B signaling pathway. More importantly, the 16S ribosomal RNA gene sequencing results indicate that post-oral of ZnPBA@YCW can effectively regulate gut microbiota by enhancing the bacterial richness and diversity, significantly increasing the abundance of probiotics with anti-inflammatory phenotype while downgrading pathogenic *E. coli* to the same level as normal mice. Such a novel nanomedicine provides a new idea for efficient treating those ROS-mediated diseases accompanying with flora disorders.

1. Introduction

Inflammatory bowel disease (IBD) is a growing global health concern characterized by chronic non-specific inflammation that can affect any part of the gastrointestinal tract, and may lead to colorectal cancer [1,2]. It consists of two major subtypes: the ulcerative colitis (UC) and Crohn's disease (CD), both of which cause symptoms such as persistent diarrhea, hematochezia, and weight loss. Current clinical treatments, including anti-inflammatory drugs, corticosteroids, and biological agents, only alleviate symptoms but are not effective in suppressing the disease progression and are associated with severe side effects, low response rates, and high costs [3,4]. Consequently, IBD, particularly difficult-to-treat cases, severely decreases patients' quality of life and

burdens the healthcare system [5]. Therefore, it is necessary to develop novel drugs to effectively inhibit the recurrence and progression of IBD by focusing on the key pathologic factors.

Although the pathogenesis of IBD remains to be fully elucidated, the development of the disease is influenced by excessive reactive oxygen species (ROS), chronic intestinal inflammation, and disturbance of the gut microbiota [6–8]. Moreover, the elevation of several pro-inflammatory factors (TNF- α , IL-6, IL-1 β), ROS (H₂O₂, \bullet OH, \bullet O₂⁻) accumulation, and hyperactive immune cells interact with each other and are constantly amplified, which subsequently creates a vicious circle between inflammation and ROS [9–11]. Furthermore, the elevated levels of ROS can act as electron acceptors to promote anaerobic respiration and proliferation of facultative anaerobic bacteria, resulting in

Peer review under responsibility of KeAi Communications Co., Ltd.

* Corresponding author.

** Corresponding author. Nanotechnology and Intestinal Microecology Research Center, Shanghai Tenth People's Hospital, School of Medicine, Tongji University, Shanghai, 200072, PR China.

*** Corresponding author. Nanotechnology and Intestinal Microecology Research Center, Shanghai Tenth People's Hospital, School of Medicine, Tongji University, Shanghai, 200072, PR China.

E-mail addresses: qinhuanlong@tongji.edu.cn (H. Qin), zhangyang0202@tongji.edu.cn (Y. Zhang), hrchen@mail.sic.ac.cn (H. Chen).

<https://doi.org/10.1016/j.bioactmat.2024.01.016>

Received 23 November 2023; Received in revised form 16 January 2024; Accepted 16 January 2024

2452-199X/© 2024 The Authors. Publishing services by Elsevier B.V. on behalf of KeAi Communications Co. Ltd. This is an open access article under the CC BY-NC-ND license (<http://creativecommons.org/licenses/by-nc-nd/4.0/>).

Escherichia coli occupying the ecological niche in IBD [12,13]. However, the conventional use of broad-spectrum antibiotics against pathogens in IBD may disrupt the gut microbiome, exacerbate the disease, and contribute to the development of drug-resistant bacteria [14,15]. Thus, it is highly desired but still in challenges to develop a multipronged intervention strategy to scavenge the pathogenic *E. coli* at specific sites and break the ROS-inflammatory vicious cycle towards IBD.

As one of the most promising therapeutic options for IBD, rationally designed nanozymes can restore redox balance and effectively regulate intestinal flora [16]. In particular, Prussian blue-based nanozymes have attracted great interest in the treatment of ROS-mediated diseases due to their superior multiple antioxidant enzyme-like activities, easy mass-preparation, and favorable biocompatibility [17–20]. For instance, Zhao et al. developed electrostatic and size-mediated manganese Prussian blue nanozymes (MPBZs) for the treatment of IBD through ROS scavenging and anti-inflammation. Yao et al. reported curcumin-modified coordination polymers CCM-CoFe PBA, which exhibited multi-enzyme activity and the ability to polarize M2 macrophage for IBD treatment. However, most studies are primarily focused on the ROS-scavenging effects of nanomedicines for IBD treatment [21, 22], few has involved to modulate the intestinal flora by rationally designed nanozymes.

Besides, the mode of administration is also a key factor affecting IBD treatment. The main advantages of oral administration over intravenous administration include higher patient compliance, reduced pain, and lower cost [23]. Various strategies have been employed by researchers to withstand the harsh environment of oral medication in the digestive tract, such as cell membrane envelope [24], yeast microcapsules [25], and a layer by layer (LBL) coating [26]. Additionally, the residence time of the drug in the gut can be significantly increased by electrostatic targeting [27,28], hydrogen bonding forces [29], and covalent bonding [30]. Therefore, the development of orally targeted drugs with negligible side effects for IBD treatment holds significant translational clinical implications.

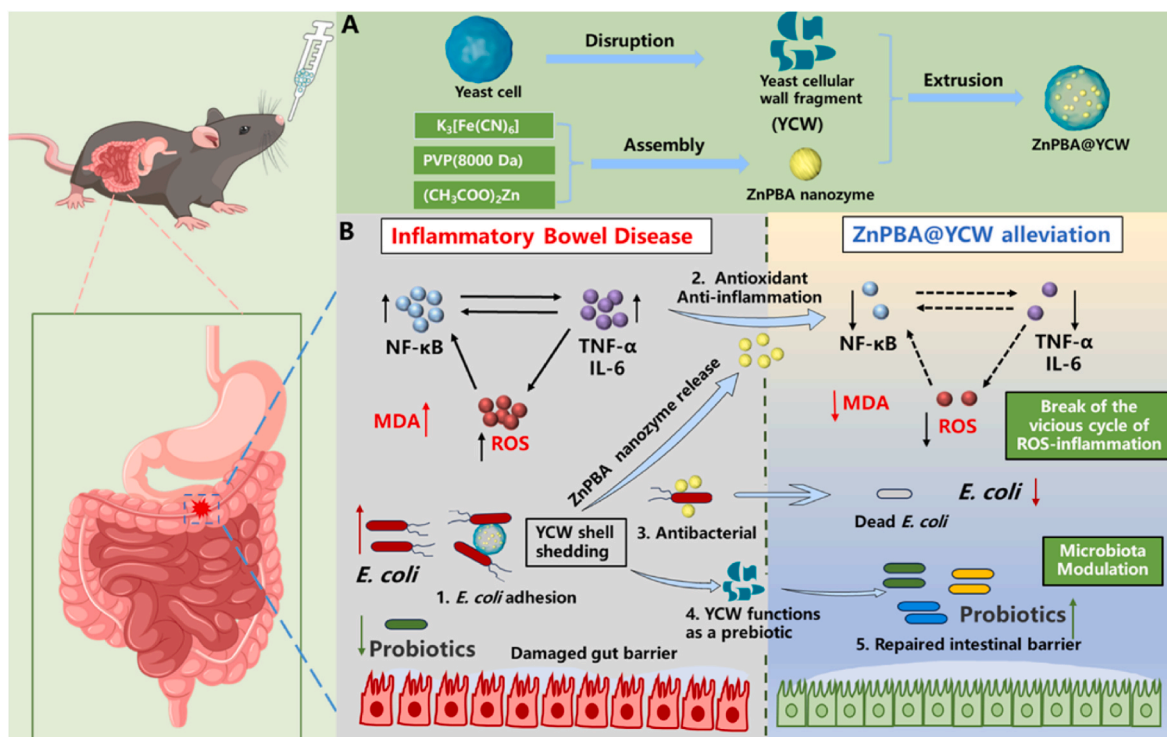
Herein, a zinc-doped Prussian blue analogue (ZnPBA) nanozyme was

synthesized by reacting $[\text{Fe}(\text{CN})_6]^{4-}$ with Zn^{2+} . Notably, the incorporation of zinc ions not only retained the multiple antioxidant enzyme activities of Prussian blue, but also endowed the ZnPBA nanozyme with antimicrobial properties, inhibition of inflammation-associated pathways, and supplementation of trace element zinc. To effectively inhibit *E. coli* at the target location, ZnPBA nanozyme was further camouflaged by yeast cellular wall (YCW) to construct enzyme-like biomimetic oral-agent ZnPBA@YCW using a simple extrusion method (Scheme 1A). After oral administration, the constructed ZnPBA@YCW could recognize and adhere to *E. coli*, which is mainly ascribed to the specific binding between the mannose-rich cell membrane of yeast cell wall and adhesion portion FimH of type 1 fimbriae in *E. coli* strains [31,32]. Moreover, the ZnPBA nanozyme was found to mitigate oxidative stress by efficiently scavenging ROS (H_2O_2 , $\bullet\text{OH}$, $\bullet\text{O}_2^-$), inhibiting the NF- κB signaling pathway, and reducing pro-inflammatory cytokines. Additionally, the oral administration of ZnPBA@YCW alleviated clinical symptoms in mice with colitis, such as diarrhea, blood in stool, and weight loss, due to the powerful antioxidant properties and the biomimetic trace element zinc supplementation of ZnPBA nanozyme. In particular, ZnPBA@YCW enhanced the diversity and richness of intestinal microbial communities, promoted the growth of probiotics, and repaired the intestinal barrier in DSS-induced colitis (Scheme 1B).

2. Results and discussion

2.1. Synthesis and characterizations of ZnPBA@YCW

The ZnPBA nanozyme was synthesized by reacting $[\text{Fe}(\text{CN})_6]^{4-}$ with Zn^{2+} under magnetic stirring. Fig. 1A and Fig. S1 show typical morphology of the prepared ZnPBA nanozyme and YCW. The X-ray diffraction pattern at the 2θ degree of 14.85, 17.08, 24.41, 28.58, 34.70, 38.87, 42.89, and 49.87° correspond well to the $\text{Zn}_3[\text{Fe}(\text{CN})_6]_2 \cdot 4/3\text{H}_2\text{O}$ (JCPDS #75–1257), indicating successful synthesis of ZnPBA nanozyme (Fig. 1B). Besides, the molar ratio of Fe/Zn in $\text{Zn}_3[\text{Fe}(\text{CN})_6]_2 \cdot 4/3\text{H}_2\text{O}$ is determined to be 0.67:1, matching well with the ICP measurement



Scheme 1. (A) Schematic illustration of the fabrication of ZnPBA@YCW. (B) Its functions including adhesion and scavenging of *E. coli*, antioxidant and anti-inflammatory, microbiota modulation and gut barrier repairment for IBD therapy.

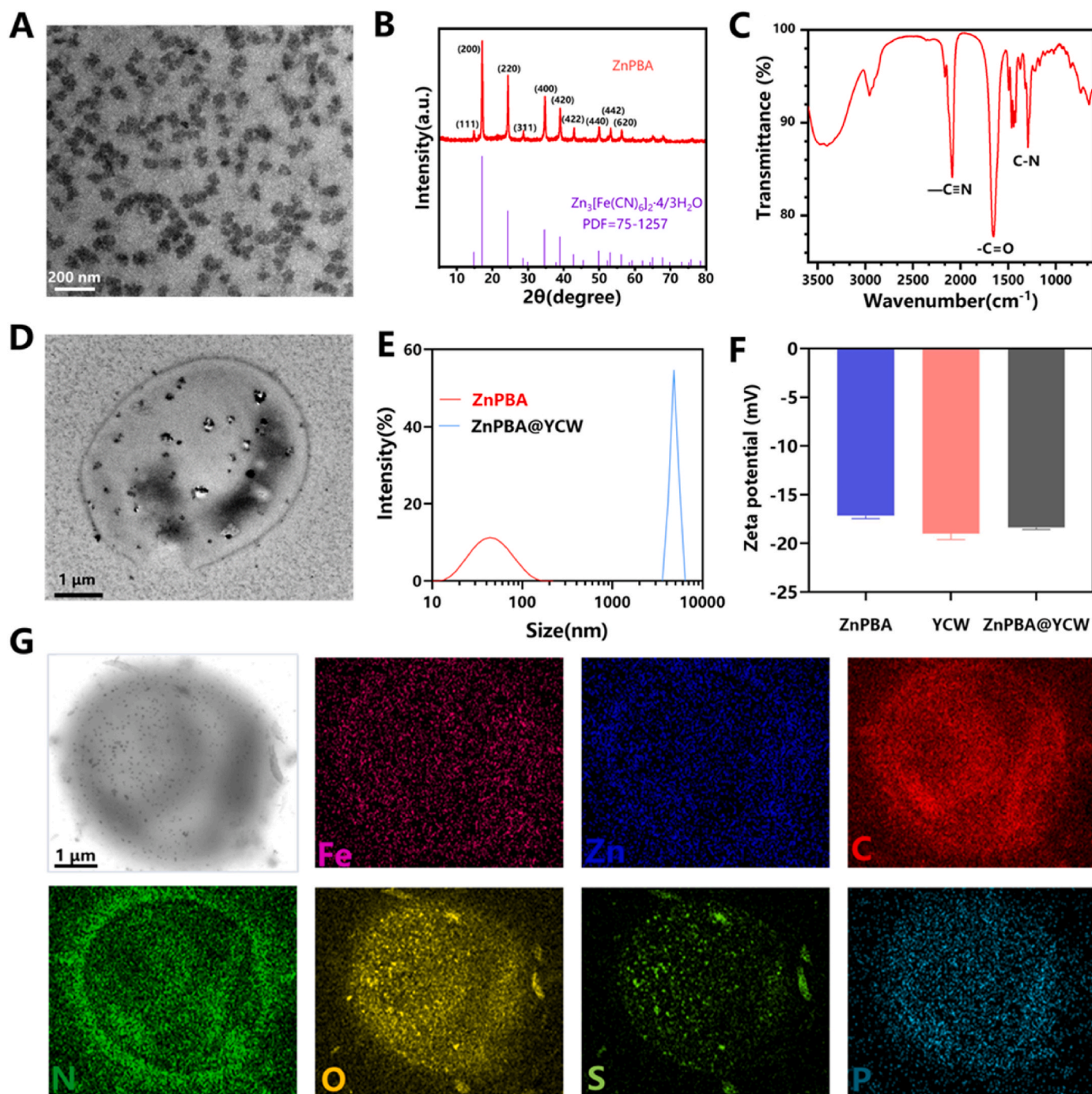


Fig. 1. Characterizations of ZnPBA nanozyme and ZnPBA@YCW. (A) Typical TEM image of ZnPBA (scale bar: 200 nm). (B) XRD pattern of ZnPBA nanozyme and standard reference of $Zn_3[Fe(CN)_6]_2 \cdot 4/3H_2O$ (JCPDS#75–1257). (C) FTIR spectrum of ZnPBA nanozyme. (D) TEM image of ZnPBA@YCW (scale bar: 1 μm). (E–F) Size distribution (E) and Zeta potential (F) changes of ZnPBA nanozyme and ZnPBA@YCW. (G) HAADF-STEM and element mapping of ZnPBA@YCW. Data in (F) are shown as mean \pm S.D. ($n = 3$).

(0.53:1) (Table S1). With regard to the FTIR spectra, the characteristic $C \equiv N$ stretching vibration occur at 2097 cm^{-1} , characteristic C–N stretching vibration occur at 1286 cm^{-1} , and the peak at 1635 cm^{-1} corresponding to $C=O$ of the PVP unit, which further confirms the successful construction of ZnPBA nanozyme (Fig. 1C).

Fig. 1D shows the typical TEM image of the prepared ZnPBA@YCW. It is clearly found that numerous ZnPBA nanoparticles are well encapsulated into the YCW, and the specific encapsulation rate of ZnPBA in YCW is calculated to be $80.4 \pm 2.4\%$. Dynamic light scattering (DLS) measurements indicate that the average hydrodynamic size of ZnPBA

nanozyme is around 43 nm, which could be enlarged to 4360 nm when they are wrapped with YCW (Fig. 1E). Besides, when encapsulated with a more negatively charged YCW, the zeta potential of ZnPBA@YCW decreases as compared to the ZnPBA nanozyme alone (Fig. 1F). The homogeneous distribution of representative elements corresponding to both ZnPBA nanozyme and YCW shown in the HAADF-STEM element mapping images (Fig. 1G) indicate successful preparation of ZnPBA@YCW.

2.2. Multienzyme-like activities and bactericidal performance of ZnPBA nanozyme

Next, the ability of ZnPBA nanozyme to scavenge ROS involved in IBD, including $\bullet\text{O}_2^-$, H_2O_2 , and $\bullet\text{OH}$ were investigated (Fig. 2A) [33]. Prior to that, the X-ray photoelectron spectroscopy (XPS) of ZnPBA nanozyme was conducted, confirming the existence of Zn, Fe, O, N elements (Fig. S2). Moreover, the valence states of iron and zinc species were analyzed by high resolution XPS spectra. In details, the peak at 707.77 eV was assigned to the Fe^{2+} , while those at 709.14 eV, 709.95 eV were attributed to Fe^{3+} (Fig. 2B). Besides, the peaks at 1020.83 and 1043.82 eV corresponded to the divalent zinc cation (Fig. 2C). These XPS spectra confirm the co-presence of divalent zinc cations and mixed +2/+3 valences of iron ions in the ZnPBA nanozyme. Afterward, the hydroxyl radical scavenging ability of ZnPBA nanozyme was assessed by monitoring the absorbance at 510 nm, corresponding to the oxidation of salicylic acid to 2,3-dihydroxybenzoic acid. As illustrated in Fig. 2D, the absorbance significantly decreased upon addition of the ZnPBA nanozyme, indicating its efficient hydroxyl radical scavenging activity. Moreover, the TiO_2/UV system was further used to investigate the effect of ZnPBA nanozyme on $\bullet\text{OH}$ elimination. As shown in Fig. 2E, the intensity of the characteristic peaks of $\text{DMPO}/\bullet\text{OH}$ decreased significantly with increasing concentration of the ZnPBA nanozyme, confirming the

efficient $\bullet\text{OH}$ scavenging ability of ZnPBA nanozyme. As an antioxidant enzyme in living organisms, superoxide dismutase (SOD) can convert superoxide anion to hydrogen peroxide and oxygen, which may open new horizons for the treatment of inflammatory diseases [34]. Therefore, the SOD-like activity of ZnPBA nanozyme was further evaluated using a SOD activity kit. As expected, the ZnPBA nanozyme exhibited efficient SOD-mimicking catalytic activity in a concentration-dependent manner (Fig. 2F). To further examine the catalase mimic activity of ZnPBA nanozyme in decomposing H_2O_2 , the O_2 production was monitored by a dissolved oxygen meter. The O_2 production gradually increased over time in a concentration-dependent manner of ZnPBA nanozyme as shown in Fig. 2G. Peroxidase is another class of antioxidant enzyme that catalyzes the reaction of substrates with hydrogen peroxide, with the latter serving as the electron acceptor [35]. When ZnPBA nanozyme was introduced to the reaction system, 3,3',5,5'-tetramethylbenzidine (TMB) was oxidized to Oxidizing-TMB, as evidenced by the specific absorbance at 652 nm, demonstrating the POD-like enzymatic activity of ZnPBA nanozyme (Fig. 2H). Furthermore, the ZnPBA nanozyme was co-incubated with *E. coli* for 12 h to evaluate their antibacterial properties by measuring the optical density at 600 nm [36]. The absorbance gradually decreased as the concentration of ZnPBA nanozyme increased, suggesting their potent antibacterial property, which was further supported by the bacterial plate cloning

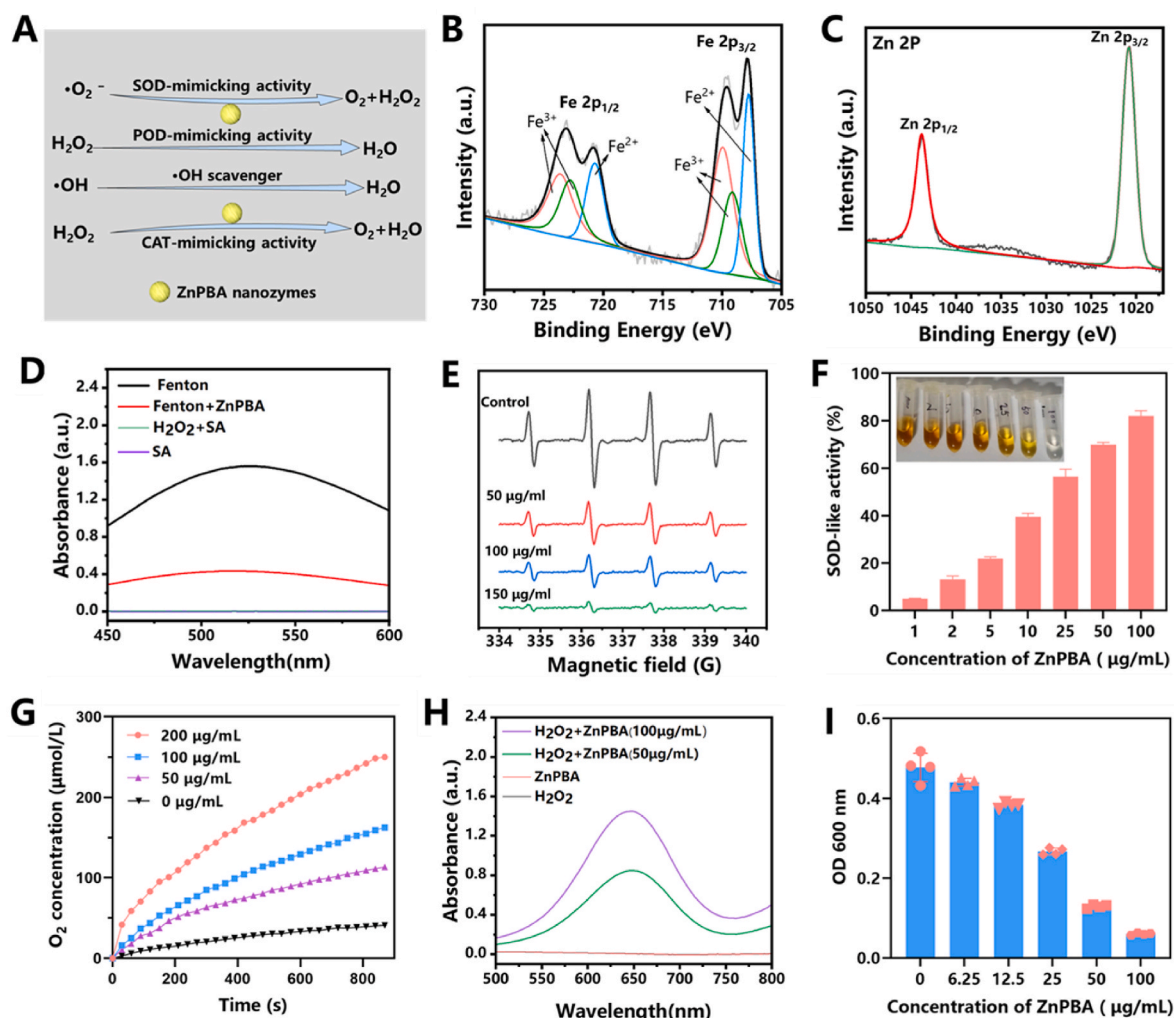


Fig. 2. ROS-scavenging and bactericidal effects of ZnPBA nanozyme. (A) Illustration of ROS scavenging by ZnPBA nanozyme. (B-C) High-resolution elemental spectra of iron (B) and zinc (C). (D-E) $\bullet\text{OH}$ scavenging activity of ZnPBA nanozyme. (F) The SOD-like activity of ZnPBA nanozyme, $n = 3$. (G) The CAT-like activity of ZnPBA nanozyme. (H) The POD-like activity of ZnPBA nanozyme. (I) Quantitative analysis of *E. coli* inhibition rates after treatment with different concentrations of ZnPBA nanozyme by measuring the optical density at 600 nm, $n = 4$. The data are presented as the mean \pm SD.

assay. (Fig. 2I and Fig. S3). The antibacterial property of ZnPBA can be attributed to the release of Zn^{2+} , which penetrates and disrupts cell membrane and flagellum (Fig. S4), thereby causing bacterial death [37]. More interesting, after 2 h of co-incubation, ZnPBA@YCW was found to adhere to *E. coli* (Fig. S5), indicating that YCW could act as a positioner to help ZnPBA nanozyme playing better roles in the local removal of *E. coli*. All the above results indicate that ZnPBA@YCW possesses efficient ROS elimination and antimicrobial properties, which holds great promise as a potential therapeutic agent for treating IBD.

2.3. Anti-oxidative and anti-inflammatory effects of ZnPBA@YCW at cellular level

Encouraged by the excellent ROS-scavenging ability of ZnPBA nanozyme, anti-oxidative and anti-inflammatory performance at cellular level of ZnPBA@YCW was further investigated (Fig. 3A). Initially, to evaluate the cytotoxicity of ZnPBA nanozyme, we conducted a CCK-8 assay by incubating the ZnPBA nanozyme with various cell types for 24 h. It is found that the cell viabilities remain above 90 % even at a concentration of 100 $\mu\text{g/mL}$, indicating the excellent cytocompatibility of ZnPBA nanozyme (Fig. 3B and S6A). Moreover, the oxidative stress in cells was demonstrated to attenuate in a concentration-dependent manner when treated with ZnPBA nanozyme alone (Figs. S6B–S6D). Therefore, the concentration of 100 $\mu\text{g/mL}$ for ZnPBA@YCW (quantification by ZnPBA) was chosen for subsequent experiments. To intuitively display the anti-oxidative performance of ZnPBA@YCW, 1 mM H_2O_2 -induced NCM460 cells oxidative damage characterized by cell live-dead staining assay was further conducted. Fig. 3C indicated numerous dead cells with red signals in the H_2O_2 group. Interestingly, after treatment with ZnPBA@YCW, the intensity of red signals reduced, confirming that ZnPBA@YCW could effectively scavenge ROS and thereby protecting cells from oxidative damage. Furthermore, quantitative analysis using CCK-8 assays demonstrated that the cell viability decreased to 52 % after treatment with H_2O_2 , but increased to 82 % when pretreated with ZnPBA@YCW (Fig. 3D). It is known that LPS can be used to induce cellular oxidative stress imbalance [38], thus an *in vitro* model of LPS-induced damage was further established using RAW264.7 cells. As expected, CCK-8 quantitative results showed that the cellular viability of RAW264.7 increased from 43 % to 87 % after treatment with ZnPBA@YCW (Fig. 3E). Additionally, the intracellular ROS level was further tested by ROS-sensitive probe 2, 7-dichlorodihydro-drofluorescein diacetate (DCFH-DA) fluorescent dye. It is found that the intracellular ROS level was significantly increased after LPS treatment. By contrast, pretreatment with ZnPBA@YCW resulted in a significant decrease in ROS-induced green fluorescence as shown in Fig. 3F, confirming its potent ROS scavenging capability. As excessive ROS-induced oxidative stress can cause the oxidation of DNA, proteins or lipids [39], thus, a lipid peroxidation kit was also used to detect the level of oxidative stress in NCM460 cells. As displayed in Fig. 3G, the intracellular malondialdehyde (MDA) content decreased significantly in the ZnPBA@YCW treatment group, demonstrating its excellent MDA alleviating ability. Collectively, all the above results indicate that ZnPBA@YCW exhibits favorable biosafety and can effectively protect cells from oxidative damage.

IBD is characterized by the excessive production of reactive oxygen species (ROS) induced by pro-inflammatory factors such as TNF- α and IL-6. In turn, ROS can activate the NF- κB signaling pathway, leading to increased secretion of pro-inflammatory factors and the formation of a ROS-inflammatory vicious cycle. Disrupting this cycle is of great interest for IBD therapy [40,41]. In this regard, we further evaluated the anti-inflammatory effect of ZnPBA@YCW by monitoring the secretion levels of TNF- α and IL-6 in an inflammation model induced by LPS. As anticipated, ZnPBA@YCW significantly decreased the levels of TNF- α and IL-6 *in vitro* (Fig. 3H and I). These findings indicate that the ZnPBA@YCW exhibits exceptional antioxidant and cytoprotective properties and is able to break the ROS-inflammatory vicious cycle,

suggesting its potential for *in vivo* treatment of IBD.

2.4. The stability of ZnPBA@YCW, residence time in the intestine, as well as the release behavior of ZnPBA from ZnPBA@YCW

The stability and site-specific retention time of orally administered drugs in the gastrointestinal tract are critical for their effectiveness. To evaluate the stability of ZnPBA@YCW in the gastrointestinal tract, we initially added ZnPBA@YCW into the simulated gastric fluid (SGF, pH 1.5) for 1 h. As shown in Figs. S7A–7D, the hydrodynamic size distribution, Zeta potential, as well as morphology of ZnPBA@YCW did not change significantly after 1 h incubation in SGF, indicating its good resistance under acidic conditions. This can be attributed to the fact that the special component of YCW and the PVP-modified ZnPBA together increase the stability of ZnPBA@YCW in gastric acid [42–44].

In order to visually observe the retention time of the ZnPBA@YCW in the intestine, the colitis mice were orally administrated with Cy5.5-labeled ZnPBA@YCW, and the mice were observed in different time points via an *in vivo* imaging system (IVIS). The results showed that fluorescent signals were still retained in the abdomen of mice 24 h after ZnPBA@YCW gavage as shown in Fig. S7E. Notably, there was still a relatively strong fluorescent intensities in the mouse colon tract 24 h later, demonstrating a relatively long retention time of ZnPBA@YCW in the intestine. Afterward, the release behavior of ZnPBA from ZnPBA@YCW was investigated. It is found that ZnPBA has a specific absorption peak at 417 nm, based on which a standard curve can be fitted (Figs. S7F–7G). The release profile of ZnPBA from ZnPBA@YCW in a simulated intestinal fluid (SIF, pH 6.8) environment shown in Fig. S7H indicated that ZnPBA gradually increased with time, and reached more than 80 % when incubated for 8 h in SIF. All the above results verify that ZnPBA@YCW can smoothly pass through the gastrointestinal tract and gradually release ZnPBA nanozyme in the inflamed colon, demonstrating its potential as a bionic oral agent for the treatment of IBD.

2.5. Therapeutic efficacy of ZnPBA@YCW in DSS-induced mouse model of colitis

Encouraged by the above *in vitro* results, the therapeutic efficacy of ZnPBA@YCW was further investigated using a DSS-induced C57BL/6 mice IBD model. The mice were given 3 % DSS in sterile drinking water ad libitum for consecutive 7 days to establish the acute colitis model (Fig. 4A). Subsequently, the mice were randomly divided into five groups ($n = 5$): Healthy control, PBS (DSS + PBS), DSS + ZnPBA, DSS + YCW and DSS + ZnPBA@YCW. On days 7, 9, and 11, the mice were given a single oral gavage treatment. Then, the therapeutic effects of ZnPBA@YCW on colitis were assessed using various indices, including daily body weight changes, DAI score, perianal blood in stool, colon length, spleen weight, H&E staining of the colon, and histologic score. Compared to the reference groups of PBS, YCW, and ZnPBA, it was found that the ZnPBA@YCW treatment showed a longer colon length (Fig. 4B and E), absence of perianal blood (Fig. 4C), less weight loss (Fig. 4D), lower spleen weights (Fig. 4F and G), and reduced DAI scores (Fig. 4H). Moreover, histological damage scores were calculated via H&E staining of colon tissue (Table S2), which showed less infiltration of inflammatory cells, crypt structures destruction, and epithelial damage in the ZnPBA@YCW group as compared to the PBS group (Fig. 4I and J). Additionally, no significant body weight change was observed in the ZnPBA@YCW group, indicating its good biocompatibility (Fig. S8). After the final treatment, the mice with DSS-induced IBD were sacrificed and performed the liver and renal function tests, including alanine aminotransferase (ALT), aminotransferase (AST), uric acid (UA), blood urea nitrogen (BUN), and creatinine (CRE) levels, which were all within the normal range (Fig. S9). Moreover, H&E staining of major organ indices reveals no noticeable histologic changes (Fig. S10). It is worth mentioning that the ZnPBA group also demonstrated a significant therapeutic effect as compared to the PBS and YCW groups, suggesting

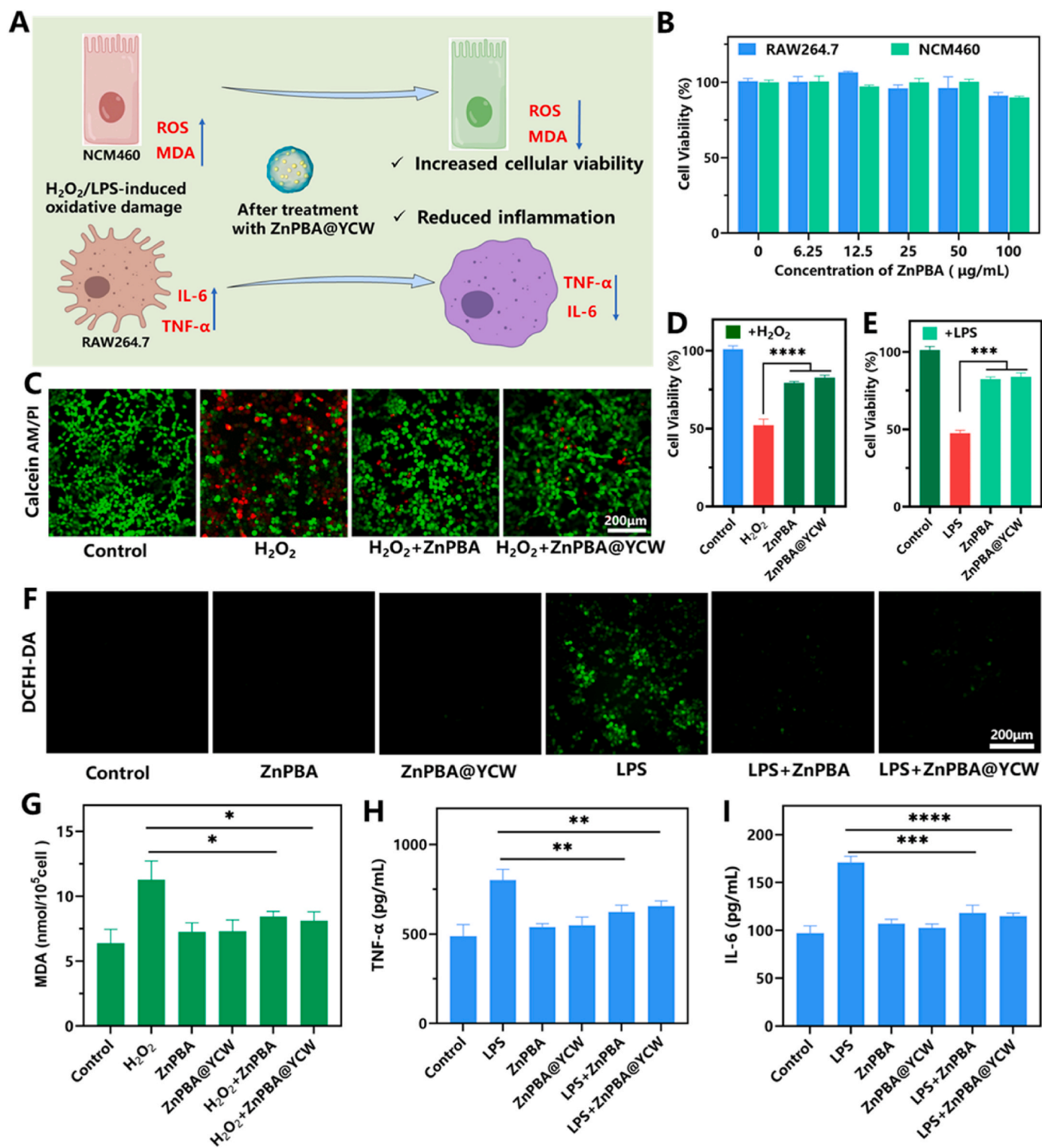


Fig. 3. Anti-oxidative and anti-inflammatory effects of ZnPBA@YCW at cellular level. (A) Schematic illustration about cytoprotection and anti-oxidative performance of ZnPBA@YCW *in vitro*. (B) Cell viabilities of cells were incubated with ZnPBA nanozyme with different concentrations for 24 h. (C) CLSM images analysis of NCM460 cells stained with Calcein-AM/PI (1 mM H₂O₂). (D) ZnPBA@YCW protected NCM460 cells from the oxidative stress caused by H₂O₂. (E) ZnPBA@YCW protected RAW264.7 cells from the oxidative damage caused by LPS. (F) CLSM images analysis of RAW264.7 cells stained with DCFH-DA. (G) MDA content. (H-I) TNF-α and IL-6 levels of RAW264.7 cells after different treatments. The data are presented as the mean ± SD, n = 4. Statistical analysis was performed using Student's two-sided *t*-test. **p* < 0.05, ***p* < 0.01, ****p* < 0.001, and *****p* < 0.0001 represented different statistical significances.

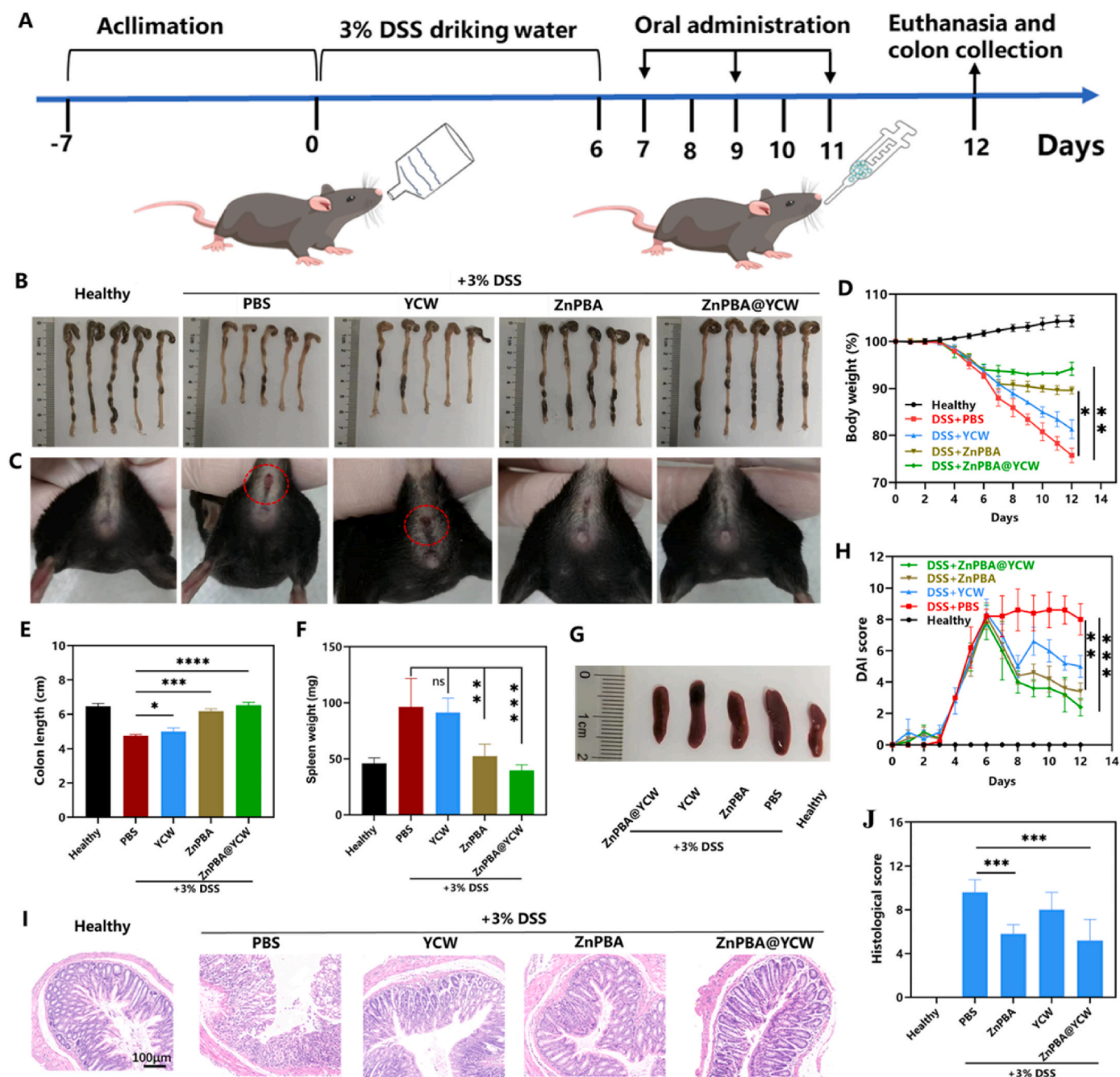


Fig. 4. ZnPBA@YCW ameliorates DSS-induced colitis. (A) Experimental protocol for acclimatization and treatment. (B) Corresponded colon photographs. (C) Representative photographs of feces. (D) Daily changes of body weight. (E) Statistical analysis of colon lengths. (F) Spleen weight. (G) Macroscopic spleen appearance. (H) Disease activity index (DAI) scores. (I) Representative images of H&E. (J) Colonic histological damage scores. The data are presented as the mean \pm SD, $n = 5$. Statistical analysis was performed using Student's two-sided t -test. * $p < 0.05$, ** $p < 0.01$, *** $p < 0.001$, and **** $p < 0.0001$ represented different statistical significances. ns stands for no significant difference.

that ZnPBA@YCW was mainly dependent on the intrinsic powerful antioxidant properties and biomimetic trace element zinc supplementation of component ZnPBA nanozyme to alleviate the symptoms of IBD [45]. Taken together, the above *in vivo* results indicate that orally administered ZnPBA@YCW exhibits excellent therapeutic effects and good biosafety on a murine model of DSS-induced colitis.

2.6. Therapeutic mechanisms for IBD

Myeloperoxidase (MPO) activity is an indicator of oxidative stress in tissues [46]. As shown in Fig. 5A and Fig. S11A, the MPO activity in the

colon tissues of mice treated with ZnPBA@YCW reduced significantly as compared to PBS group. Additionally, the levels of MDA, a marker of lipid peroxidation, were significantly lower in the ZnPBA@YCW group as compared to the PBS group, indicating a reduction in oxidative damage in the inflamed colon (Fig. 5B). These results suggest that ZnPBA@YCW can alleviate colitis by reducing oxidative damage.

The NF- κ B signaling pathway, which involves the production of pro-inflammatory cytokines such as TNF- α , IL-6, and IL- β , has been reported to be closely relative to the pathogenesis of IBD [47]. Therefore, the rational design of nanozymes to effectively inhibit NF- κ B signaling pathway is a promising strategy for IBD treatment. Numerous studies

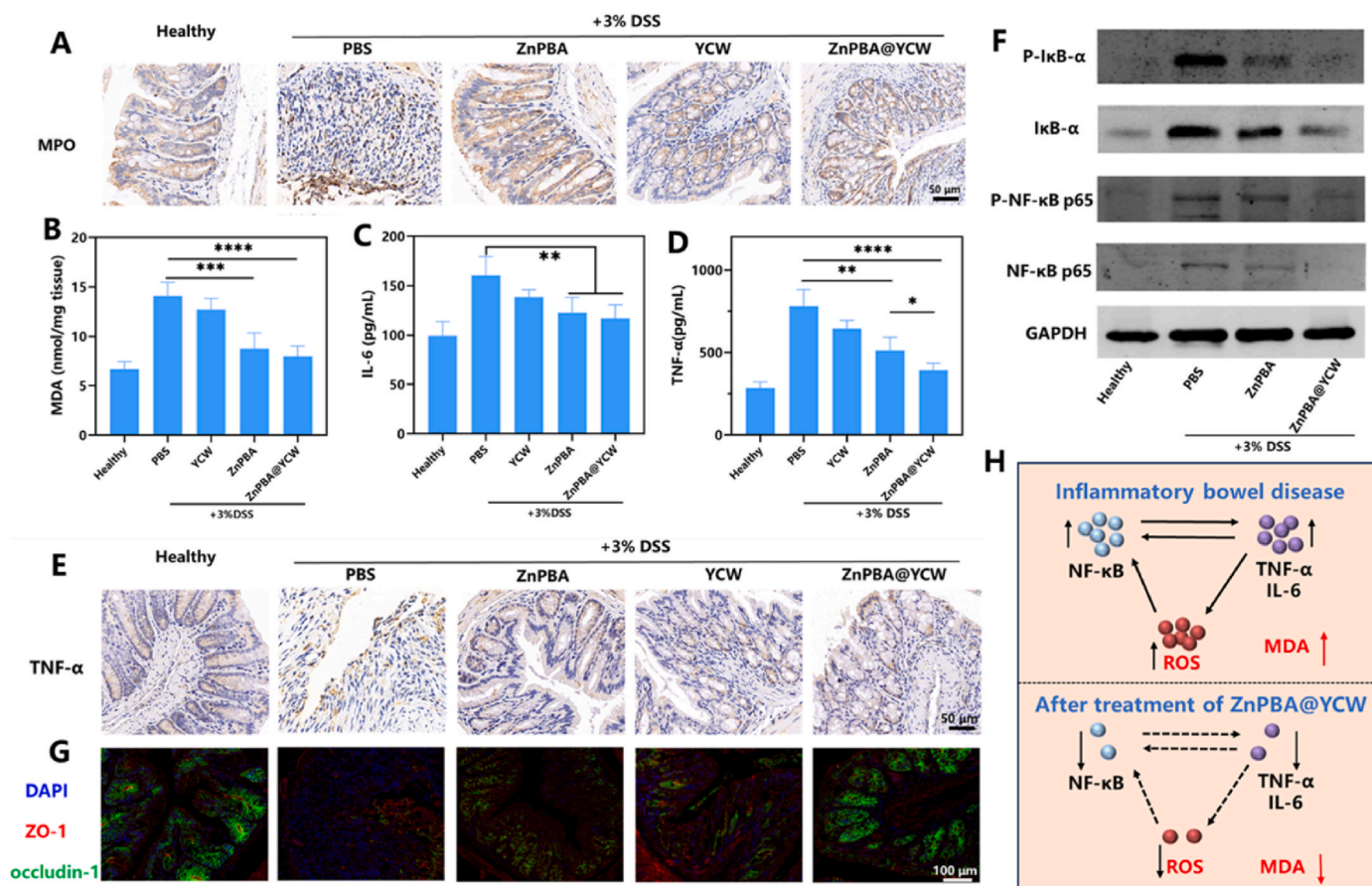


Fig. 5. Therapeutic mechanisms of ZnPBA@YCW on IBD. (A) Representative images of MPO staining. (B) MDA level. (C–D) IL-6 and TNF- α expression levels. These data are presented as the mean \pm SD, $n = 5$. (E) Representative images of TNF- α staining. (F) Western blot analysis of the expression of phospho-NF- κ B p65 (P-NF- κ B p65), total NF- κ B p65, phospho-I κ B- α (P-I κ B α), and total I κ B α in colon tissues. (G) Immunofluorescence staining for the tight junction proteins ZO-1 (red), occludin-1 (green), DAPI (blue). (H) Schematic illustration of ZnPBA@YCW breaks the vicious cycle of ROS-inflammation. Statistical analysis was performed using Student's two-sided t -test. $^{*}p < 0.01$, $^{**}p < 0.001$, and $^{***}p < 0.0001$ represented different statistical significances. ns stands for no significant difference.

have demonstrated that zinc ions exert antioxidant and anti-inflammatory effects by inhibiting the NF- κ B signaling pathway [48]. In addition, zinc deficiency is strongly associated with impaired intestinal barrier function, aggravated intestinal inflammation, disturbance of the gut microbiota and poor clinical prognostic outcomes in IBD [49–51]. To investigate the mechanism of ZnPBA@YCW exerts its anti-inflammatory effects in the DSS-induced IBD model, immunohistochemistry and ELISA assays were used to determine the secretion of inflammatory factors. As expected, the ZnPBA@YCW can significantly reduce the secretion of TNF- α and IL-6 in colonic tissue and serum as compared to the DSS + PBS group (Fig. 5C–E, Figs. S11B and S12), demonstrating its excellent ability to relieve colitis and systemic inflammation. Besides, anti-inflammatory factors IL-10 expression in colonic tissue was found to be elevated by ZnPBA@YCW treatment (Fig. S13). Additionally, the key proteins of the colon tissue were further determined by Western blot assays. As shown in Fig. 5F, compared to the DSS + PBS group, the expression of phosphorylated NF- κ B p65 and I κ B- α proteins was significantly reduced in the ZnPBA@YCW group, indicating that the NF- κ B signaling pathway was severely inhibited.

Zonula occluden-1(ZO-1) and Occludin-1 are intercellular tight junction proteins that reflect the intestinal mechanical barrier, which could prevent harmful bacteria, viruses, toxins, etc [52]. Furthermore, representative immunofluorescence images revealed that the mice treated with ZnPBA@YCW exhibited improved intestinal epithelial barrier repair (Fig. 5G), which could be attributed to the fact that zinc promotes the expression of ZO-1 and occludin-1 by inhibiting NF- κ B [53]. Overall, in addition to conferring antimicrobial properties to

ZnPBA nanozyme, the zinc ion incorporation was effective in inhibiting the NF- κ B signaling pathway and promoting the repair of the intestinal epithelial barrier. Collectively, these results demonstrate that ZnPBA@YCW can effectively break the vicious cycle between ROS and inflammation to restore redox balance and maintain intestinal homeostasis (Fig. 5H). Importantly, the therapeutic efficacy of ZnPBA@YCW group was superior to that of the ZnPBA group, highlighting the significant role of YCW.

2.7. Modulation of gut flora

A growing body of researches have shown that disturbance in the gut microbiota and their metabolites significantly affect the onset and development of IBD [54,55]. In order to reveal the effect of ZnPBA@YCW on the modulation of gut microbiome, a high-throughput 16S ribosomal RNA (rRNA) gene sequencing of the V3–V4 regions was conducted to examine the alterations in the microbial community. The analysis of α -diversity revealed that the richness (Observed OTUs) and diversity (Shannon, Simpson, Chao, ACE) of the microbiome notably increased in the ZnPBA@YCW treatment group compared to those in the PBS group of DSS-induced colitis mice (Fig. 6A–C and Fig. S14). Moreover, β -diversity analysis using nonmetric multidimensional scaling (NMDS) plots showed that the bacterial community structures in the ZnPBA@YCW treatment group were very similar to those of healthy mice, whereas the community structures of colitis mice treated with PBS were distinct (Fig. 6D), which was consistent with the Principal Co-ordinates Analysis (Fig. S15). Next, the bacterial community

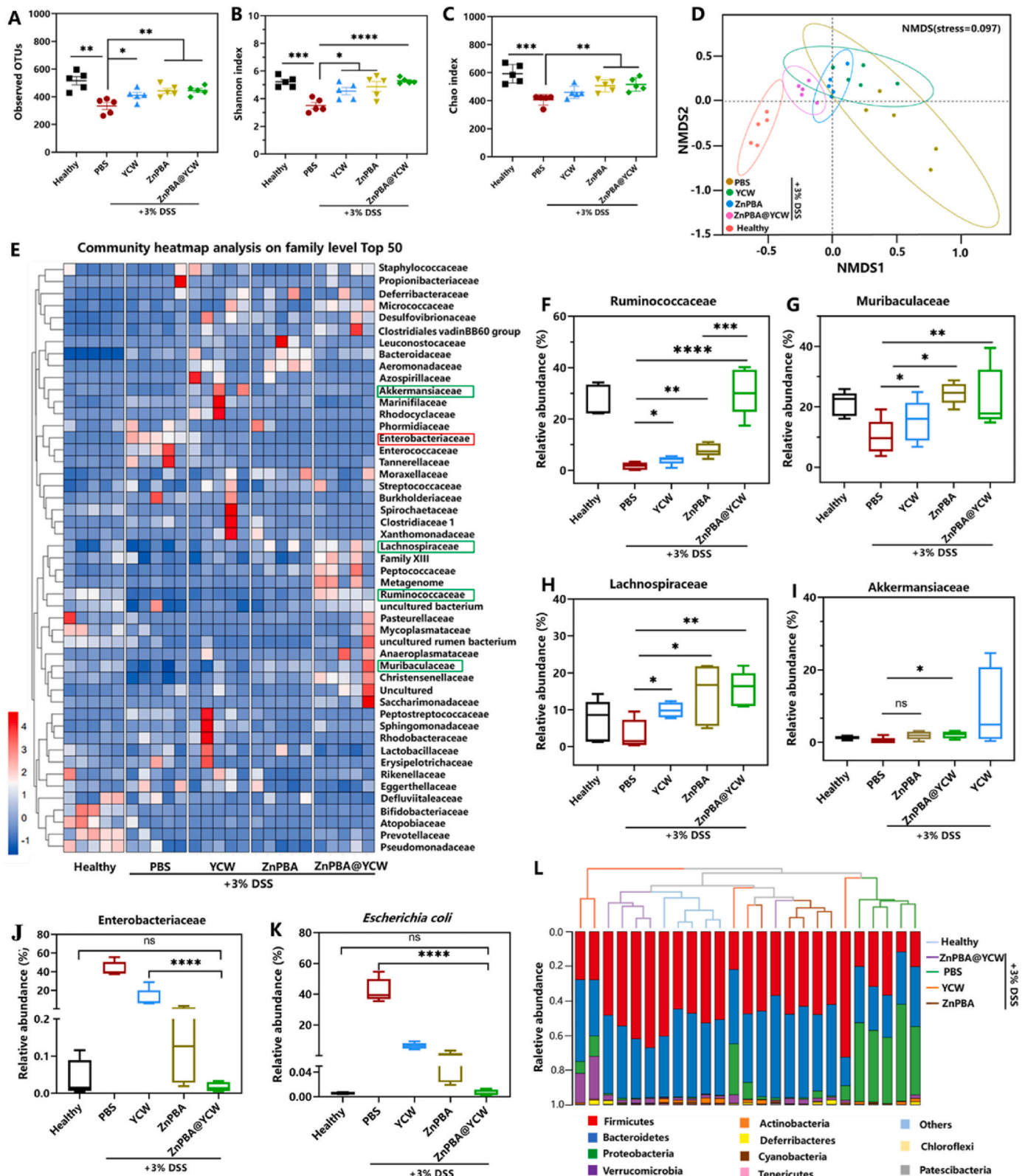


Fig. 6. ZnPBA@YCW modulates gut microbiota. (A–C) Alpha diversity displayed by observed OTU, Shannon index, and Chao index. (D) NMS2 (nonmetric multi-dimensional scaling) plot analysis of the gut microbiome β -diversity. (E) Heatmap of the relative abundance of the 50 most abundant family-level taxa. (F–K) Relative abundance of select taxa. (L) UPGMA clustering tree and community structure histograms. These data are presented as the mean \pm SD, $n = 5$. Statistical analysis was performed using Student’s two-sided t -test. * $p < 0.05$, ** $p < 0.01$, *** $p < 0.001$, and **** $p < 0.0001$ represented different statistical significances. ns stands for no significant difference.

composition of the mice after treatment was further examined at the phylum and family level in detail. The IBD is obvious with microbial signatures of dysbiosis at the phylum level, characterized by the increased relative abundance of Proteobacteria and reduced abundance of Firmicutes. Interestingly, after different interventions, the ZnPBA@YCW group significantly increased the relative abundance of Firmicutes and decreased the relative abundance of harmful Proteobacteria in DSS-colitis mice, whereas the PBS group further aggravated the dysbiosis in IBD (Fig. S16). Especially, the abundance of probiotics including Ruminococcaceae, Muribaculaceae and Lachnospiraceae was broadly expanded after treatment with ZnPBA@YCW (Fig. 6E–H and Fig. S17), which is much contributed to promote dietary fiber fermentation to produce the short-chain fatty acids (SCFAs) [56–58]. SCFAs are crucial bacterial metabolites for the maintenance of immune homeostasis, inhibiting pathogen colonization, and ameliorating intestinal inflammation [59]. Furthermore, Ruminococcaceae can metabolize primary bile acids into secondary bile acids, which also helps reduce intestinal inflammation [60]. Besides, Akkermansia, a next-generation probiotic that contributes to maintaining gut barrier function and limiting intestinal inflammation, was also increased markedly in the ZnPBA@YCW group (Fig. 6I) [61]. Of note, consistent with a previous study, our research also demonstrated that YCW could promote the growth of a variety of probiotics such as Muribaculaceae, Lachnospiraceae, Ruminococcaceae, Lactobacillaceae (Fig. 6F–H and Fig. S18) [42]. Additionally, it is known that ROS can act as electron acceptors to promote anaerobic respiration and expansion of facultative anaerobic bacteria such as Enterobacteriaceae in IBD, leading to dysbiosis of the gut microbiota [62,63]. Consequently, these abnormally enhanced IBD-associated *E. coli* has the ability to adhere to and invade epithelial cells, induce cell death in dendritic cells and stimulate the release of the proinflammatory cytokines such as TNF- α , IL-6, and IL-23 [64]. In order to visually observe the adhesion capability of ZnPBA@YCW to *E. coli*, a zebrafish model of bacterial infection was established. The zebrafish was firstly incubated in fresh medium for 2 h with 10^7 CFU *E. coli* expressing green fluorescent protein (GFP), then infected zebrafish were incubated with ZnPBA@YCW for 1.5 h. As expected, it is found that ZnPBA@YCW can well recognize and adhere to *E. coli* in zebrafish (Fig. S19). Afterward, accompanying with gradual degradation of YCW [65], the released ZnPBA nanozyme works to kill *E. coli* through disrupting the cell membrane. More interestingly, as shown in Fig. 6J and K, the abundance of Enterobacteriaceae and *E. coli* in the ZnPBA@YCW group was significantly down-regulated and restored to levels equivalent to those in the healthy group. Furthermore, the linear discriminant analysis (LDA) effect size (LEfSe) analysis shown in Fig. S20–S21 confirmed a clear enrichment in the abundance of the aforementioned probiotics in the ZnPBA@YCW group, while the abundance of Enterobacteriaceae and *Escherichia shigella* pathogens was significantly increased in colitis mice (LDA (\log_{10}) > 2.0). Moreover, the Unweighted Pair Group Method with Arithmetic Mean (UPGMA) clustering analysis results revealed that ZnPBA@YCW treatment and the healthy group had the closest community composition, demonstrating the superior recovery of the gut microbiota. Notably, although ZnPBA or YCW group has some effects on the intestinal flora of IBD mice, the gut microbiota composition still rarely cluster with the healthy group, indicating that the effect of ZnPBA@YCW depends on the synergistic action of YCW and ZnPBA to regulate the microbiota (Fig. 6L). Collectively, these findings confirm that ZnPBA@YCW can modulate gut flora by enhancing microbial biodiversity, promoting the growth of probiotics, and inhibiting *E. coli* involved in IBD pathogenesis.

3. Conclusion

In summary, a novel enzyme-like biomimetic oral-agent ZnPBA@YCW by camouflaging ZnPBA nanozyme with YCW was successfully synthesized for the first time, to precisely regulate gut microbiota meanwhile break the vicious cycle of ROS-inflammation for

efficiently treating IBD. After oral administration, ZnPBA@YCW could not only precisely recognize *E. coli* and release ZnPBA nanozyme to eliminate *E. coli* at special position of inflamed colon, but also boost the beneficial bacteria expansion. Specifically, the ZnPBA nanozyme was found to restore redox homeostasis by effectively scavenging ROS to reduce lipid peroxidation, inhibiting the NF- κ B signal pathway, and decreasing the secretion of inflammatory factors TNF- α and IL-6, which was beneficial to alleviate IBD symptoms. More importantly, the 16S ribosomal RNA gene sequencing results indicate that ZnPBA@YCW can successfully modulate gut microbiota through increasing the bacterial diversity and richness, reducing the pathogenic *E. coli* to the normal level, and enhancing the abundance of Akkermansia and the SCFAs-producing probiotics (e.g., Muribaculaceae, Lachnospiraceae, Ruminococcaceae) in a DSS-induced mouse model. Moreover, ZnPBA@YCW could repair the intestinal epithelial barrier in mice with enteritis and demonstrated a favorable biosafety profile. Encouragingly, considering that ROS-mediated diseases such as Parkinson, rheumatoid arthritis, and gout are also strongly associated with disturbances in the intestinal flora, our therapeutics may provide a good paradigm for treating these diseases.

4. Materials and methods

4.1. Materials

Poly(vinylpyrrolidone) (PVP, 8000Da), potassium ferricyanide ($K_3[Fe(CN)_6]$), and zinc acetate dihydrate were obtained from Sinochem Chemical Reagents (Shanghai, China). Yeast cells (Angel, commercially) Dingguo Biotechnology Co., Ltd. (China). Fetal bovine serum (FBS), Cell Counting Kit-8 (CCK-8), 2,7-dichlorodihydrofluorescein diacetate (DCFH-DA), 5,5-dimethyl-1-pyrroline-N-oxide (DMPO), calcein acetoxyethyl ester (Calcein-AM), and propidium iodide (PI) were purchased from Shanghai Qihai Futai Biotechnology (Shanghai, China). 3,3',5,5'-Tetramethylbenzidine (TMB) and salicylic acid (SA) were supplied by Beyotime Biotechnology Co., Ltd. (Shanghai, China). NF- κ B p65 Antibody, Phospho-NF- κ B p65 Antibody, I κ B alpha Antibody, Phospho-I κ B-alpha Antibody, GAPDH Rabbit pAb were acquired from Abclonal (Hubei, China).

4.2. Characterization

Transmission electron microscopy (TEM) images were obtained on a JEM-2100F TEM (JEOL Ltd., Japan). The morphology and elemental mapping of the ZnPBA@YCW were observed by scanning electron microscopy (SEM, Quattro S, ThermoFisher Scientific, USA). Hydrodynamic diameter and ζ -potential were measured by a Zetasizer Nanoseries (DLS, Malvern, UK). Powder X-ray diffraction (XRD) patterns were investigated by a Rigaku D/Max 2200 PC diffractometer with the 2θ ranging from 10° to 80° . X-ray photoelectron Spectroscopy (XPS) analysis was conducted on a Thermo ESCALAB250 (USA). UV–vis spectra were obtained on a Shimadzu UV-3600 spectrophotometer (Shimadzu, Japan). Fourier Transform Infrared (FTIR) spectra were performed on a Bruker Vertex 70 FTIR spectrometer (Germany). The element analysis was determined on an Agilent 715 ICP-OES (Thermo Fisher Scientific, USA). Electron Paramagnetic Resonance (ESR) spectra were obtained on a Bruker ESR 5000 (Germany). Confocal laser scanning microscope (CLSM) images were used to evaluate the cell viability and ROS scavenging ability (FV1000, Olympus, Japan).

4.3. Design and preparation of ZnPBA nanozyme and ZnPBA@YCW

To synthesize ZnPBA nanozyme, 0.04 mmol $K_4[Fe(CN)_6]$, and 0.3 g PVP were dissolved into 10 mL deionized water under magnetic stirring for 10 min (recorded as solution A). Similarly, 0.06 mmol Zinc acetate dihydrate were dispersed into 10 mL distilled water under magnetic stirring for 10 min (recorded as solution B). Solution B was then added

slowly to solution An under magnetic stirring for 6 min, and the mixture solution was stored statically at room temperature for 6 h. Then, the nanozyme was further washed several times using ultrafiltration tubes (MWCO = 50 kDa). ZnPBA nanozyme was stored in refrigerator at 4 °C for backup. The extraction of YCW was carried out according to a previously reported method [66]. Finally, the ZnPBA@YCW was constructed by extruding by liposome extrusion apparatus (Avanti).

4.4. Characterization of hydroxyl radical scavenging capacity

- (1) ESR: A quartz glass dish was composed of 50 μL solution system containing 200 $\mu\text{g}/\text{mL}$ TiO_2 , 5 μL DMPO and different concentrations of ZnPBA nanozyme (0, 50, 100, 150 $\mu\text{g}/\text{mL}$). Subsequently, the appeal system was tested on the machine after irradiation with UV lamp under dark condition for 5 min.
- (2) The salicylic acid (SA) method was also used to evaluate the $\cdot\text{OH}$ scavenging activity. Typically, 3 mM H_2O_2 and 2 mM FeSO_4 were mixed to produce $\cdot\text{OH}$, followed by the addition of ZnPBA nanozyme. After 1 h, SA (2 mM) was added to the above reaction system and the remaining amount of $\cdot\text{OH}$ was determined by detecting the absorbance value at 510 nm.

4.5. CAT-like activity assessment

The detections were performed in a pH 7.4 solution containing, 10 mM H_2O_2 and different concentrations of ZnPBA nanozyme (0, 50, 100, 200 $\mu\text{g}/\text{mL}$). Then, the O_2 concentration at different time points was monitored by a portable dissolved oxygen meter (JPBJ-610L, Rex, INESA Scientific Instrument).

4.6. SOD-like activity assessment

The $\cdot\text{O}_2^-$ scavenging activity of ZnPBA nanozyme was measured through the inhibition of water-soluble formazan formation generated from WST-8 using a colorimetric SOD assay kit under the instructions of manufacturer (Cat No. S0101, Beyotime).

4.7. POD-like ability evaluation

4 mM H_2O_2 solution with 1 mM TMB and ZnPBA nanozyme were added into the colorimetric dish. The absorbance at 652 nm was immediately recorded using a UV-3600 spectrophotometer.

4.8. In vitro antibacterial experiment

The antibacterial properties of ZnPBA nanozyme were tested by co-incubating different concentrations of ZnPBA nanozyme with *Escherichia coli* (DH 5 α) in LB liquid medium. The OD value at 600 nm was measured at predetermined time points using a microplate reader (BioTek, China), and the remaining bacteria were collected into blood agar plate for bacterial colony counting.

4.9. Cell cultures

RAW264.7, HUVEC, CT26, and NCM460 cells were cultured in High-Glucose Dulbecco's Modified Eagle's Medium (HDMEM) containing 1 % penicillin G sodium/streptomycin sulfate and 10 % FBS. All cells were cultured in T-25 flasks or dish for cell reproduction at 37 °C and 5 % CO_2 in an incubator.

4.10. Cell toxicity

The cells were incubated with ZnPBA nanozyme at different concentrations (0, 6.25, 12.5, 25, 50, 100 $\mu\text{g}/\text{mL}$) for 24 h. Afterward, the medium was discarded and the cells were washed with PBS twice. Then, the culture medium was replaced with free-FBS medium containing

CCK-8 reagent (10:1) and co-cultured with the pre-treated cells for 1 h in the incubator. Finally, the absorbance was measured using a microplate reader.

4.11. In vitro cyto-protection and ROS scavenging of ZnPBA@YCW

To investigate the protective effect of ZnPBA@YCW against H_2O_2 -induced oxidative damage, Calcein-AM and PI are used to visualize the live and dead cells. The cells were seeded in confocal dish and incubated for 24 h. Then, the medium was replaced with fresh media containing 100 $\mu\text{g}/\text{mL}$ ZnPBA@YCW and 1 mM H_2O_2 . After 6 h, the cells were stained with Calcein-AM and PI, and observed using a CLSM. The corresponding CCK-8 assay results were obtained as described above.

2',7'-Dichlorofluorescein diacetate (DCFH-DA) was used to evaluate the intracellular total ROS levels. Briefly, RAW264.7 cells were seeded in a confocal dish and incubated for 24 h, followed by incubation with 2 mL ZnPBA@YCW (100 $\mu\text{g}/\text{mL}$) for 6 h. Then, LPS (1 $\mu\text{g}/\text{mL}$) was incubated with cells for 12 h. Afterward, the cells were incubated with 1 mL DCFH-DA (10 μM in serum-free medium) for another 30 min. After that, the cells were washed with serum-free medium thrice to remove unloaded DCFH-DA probe, the cells were then imaged using a CLSM. RAW264.7 cells were further seeded into 96-well plates and incubated for 24 h. Subsequently, ZnPBA and ZnPBA@YCW in HDMEM medium were added to the wells respectively and incubated for 6 h. Afterward, the medium was replaced with fresh HDMEM containing LPS (6.4 $\mu\text{g}/\text{mL}$) for another 12 h. Finally, the cell viability was determined using standard CCK-8 assays.

4.12. Measurements of cytokines

To determine the anti-inflammatory ability of ZnPBA@YCW at the cellular level, 1 $\mu\text{g}/\text{mL}$ LPS-pretreated RAW264.7 cells were incubated with 100 $\mu\text{g}/\text{mL}$ ZnPBA@YCW for 12 h. The ELISA assay was conducted according to the manufacturer's protocol using mouse ELISA kits from Beyotime.

4.13. Intracellular lipid peroxide detection

NCM460 cells seeded onto 12-well plates. HDMEM medium containing 100 $\mu\text{g}/\text{mL}$ ZnPBA@YCW (quantification by ZnPBA) were cocultured with NCM460 cells for 7 h. Then, all the wells were treated by the addition of H_2O_2 (1 mM) and incubated for another 12 h. After that, the cell lysis solution was added to the wells and incubated for 30 min. The supernatant was collected by centrifugation (10000 g, 8 min), and the MDA level of the cell lysis supernatant was measured using MDA detection kit from Beyotime.

4.14. ZnPBA@YCW adhesion to E. coli

Firstly, the 120 hpi zebrafish were soaked in the 10^7 CFU *E. coli* solution for 2 h. Then Zebrafish were washed with a fresh Embryo Culture Medium twice and co-incubated with ZnPBA@YCW for 1.5 h at 28 °C. Following incubation, the zebrafish were washed with a fresh medium twice and placed in a confocal dish for CLSM imaging.

4.15. Efficacy for treatment of murine colitis

All the animal experiments were performed with the approval of the Tongji University Experimental Animal Center, and the animal biomedical research authorization number is TJLAC-020-228. Mice were housed under specific pathogen-free conditions on a 12-h light/dark cycle and fed standard mouse chow ad libitum. C57BL/6 mice (female, 6 weeks old) were randomly divided into five groups (n = 5): Healthy (PBS), PBS (DSS + PBS), DSS + YCW, DSS + ZnPBA, and DSS + ZnPBA@YCW. The mice in the DSS group were received 3 % DSS in sterilized drinking water for 7 days to induce colitis model. The Healthy

and PBS groups were treated with 200 μ L PBS, while the other groups were orally administered with YCW, ZnPBA (200 μ g/mL, 200 μ L), and ZnPBA@YCW (200 μ g/mL, 200 μ L) on predetermined days. The mice were weighed daily and Disease Activity Index (DAI) was recorded. Stool samples were collected on day 12, then the mice were euthanized, and the collected colon length and spleen weight were measured. In addition, the colon tissues were used for histological, MPO activity, epithelium barrier, Western Blot analysis, MDA detection, and inflammatory cytokine evaluations.

4.16. DAI index score

The weight change, bloody stool and diarrhea of IBD mice were observed daily. The DAI index score of mice was obtained by calculating the percentage of weight loss of mice (0 point for weight loss, 1 point for weight loss of 1 %–5 %, 2 points for weight loss of 6 %–10 %, and 3 points for weight loss of 11 %–15 %), fecal viscosity (normal score is 0 points, loose stool is 2 points, diarrhea is 4 points) and fecal bleeding (normal 0 points, occult blood 2 points, overt bleeding 4 points).

4.17. Histopathology

Colon tissue samples were fixed in a solution of 4 % paraformaldehyde and embedded in paraffin. The samples were then sectioned at 5 μ m and stained with H&E to evaluate the severity of colonic damage. Histological scores of the colon were assessed to indicate the severity of inflammation, number of crypts, and degree of ulceration (Table S2).

4.18. Immunohistochemistry

To detect MPO and TNF- α , formalin-fixed paraffin-embedded (FFPE) tissue sections were deparaffinized using xylene and a graded ethanol series (100 %, 85 %, and 75 %). The Slides were washed with PBS three times and then immersed in citric acid buffer (pH 6.0) and incubated in a microwave oven for 15 min for antigen retrieval. After cooling naturally, the slides were washed with PBS (pH 7.4) three times for 5 min each. An appropriate amount of endogenous peroxidase blocking buffer was dropped onto the slides and incubated at room temperature for 10 min to block the endogenous peroxidase in the tissues. The Slides were then blocked with 3 % BSA at room temperature for 30 min to avoid nonspecific binding and were incubated with anti-MPO (1:1000) overnight at 4 $^{\circ}$ C, followed by washing three times with PBS. Subsequently, the slides were incubated with the secondary HRP peroxidase-conjugated Goat Anti-Mouse IgG for 50 min at room temperature in the dark. Finally, the sections were stained with 3,3'-diaminobenzidine (DAB) as a chromogen and counterstained with hematoxylin.

4.19. Immunofluorescence

To detect the expression of ZO-1 and occludin-1, the colon sections were subjected to antigen retrieval and blocking, incubated with diluted primary antibodies (1:1000) in 1 % BSA in PBST overnight at 4 $^{\circ}$ C. After that, they were incubated with secondary CoraLite488-conjugated Goat Anti-Rabbit IgG for 50 min at room temperature in the dark. Slides were washed three times with PBS and stained with DAPI solution at room temperature for 10 min. Subsequently, the residual solution was removed slightly, and the coverslips were added with mounting medium.

4.20. Western blot analysis

Proteins from colon tissues in different treatment groups were extracted and quantified by BCA Concentration protein Assay Kit (Beyotime). The proteins were boiled in loading buffer, separated by 10 % SDS-PAGE, and transferred to a PVDF membrane. The proteins were

blocked with 5 % bovine serum albumin for 15 min at room temperature, and primary antibodies (IkB- α , 1:2000; P-IkB- α , 1:2000; NF- κ B p65, 1:1000; P-NF- κ B p65, 1:1000; GAPDH, 1:5000) were added and incubated overnight at 4 $^{\circ}$ C. After washing three times with TBST, the blots were incubated with IRDye® 680RD Donkey anti-Mouse IgG Secondary Antibody for 1 h at room temperature. The immunoreactive blots were observed using a biofluorescence system system (Odyssey).

4.21. 16S gene sequencing and analysis

Feces from each mouse were collected in autoclaved sterile tubes on day 12 and stored at – 80 $^{\circ}$ C. The 16S gene sequencing and analysis were conducted at Shanghai Applied Protein Technology. Total genome DNA from samples was extracted using CTAB/SDS method and sequenced by building a sequencing library on the Illumina HiSeq 6000 platform. Finally, data analysis was performed on APT-BioCloud.

4.22. Statistical analysis

Data were analyzed by unpaired Student's two-sides *t*-test using GraphPad Prism 9.0 software and IBM SPSS Statistics v.23.0. All values are reported as mean \pm SD with the indicated sample size. **p* < 0.05, ***p* < 0.01, ****p* < 0.001, and *****p* < 0.0001 represented different statistical significances. ns stands for no significant difference.

Ethics approval

All the animal experiments were performed with the approval of the Tongji University Experimental Animal Center and all procedures were performed according to the guidelines and animal welfare protocols. The animal biomedical research authorization number is TJLAC-020-228.

CRediT authorship contribution statement

Zhangpeng Shi: Writing – original draft, Validation, Methodology, Investigation, Formal analysis, Data curation, Conceptualization. **Xiaohong Li:** Validation, Methodology, Investigation, Formal analysis, Data curation. **Jufeng Chen:** Validation, Methodology, Investigation, Formal analysis. **Zideng Dai:** Software, Resources, Methodology, Formal analysis. **Yefei Zhu:** Software, Resources, Formal analysis. **Tan Wu:** Software, Resources. **Qing Liu:** Investigation, Methodology. **Huanlong Qin:** Writing – review & editing, Supervision, Funding acquisition, Conceptualization. **Yang Zhang:** Writing – review & editing, Supervision, Funding acquisition, Conceptualization. **Hangrong Chen:** Writing – review & editing, Supervision, Funding acquisition, Conceptualization.

Declaration of competing interest

All authors declare that there are no competing interests.

Acknowledgements

This work was supported by the National Natural Science Foundation of China (Grant Nos.32030061,32271384), Shanghai International Cooperation Project (No.23490712900) and the Basic Research Program of Shanghai Municipal Government (Grant No. 21JC1406000).

Appendix A. Supplementary data

Supplementary data to this article can be found online at <https://doi.org/10.1016/j.bioactmat.2024.01.016>.

References

- [1] G.G. Kaplan, S.C. Ng, Understanding and preventing the global increase of inflammatory bowel disease, *Gastroenterology* 152 (2017) 313–321.
- [2] A.E. Shin, Y. Tesfagiorgis, F. Larsen, M. Derouet, P.Y.F. Zeng, H.J. Good, L. Zhang, M.R. Rubinstein, Y.W. Han, S.M. Kerfoot, A.C. Nichols, Y. Hayakawa, C.J. Howlett, T.C. Wang, S. Asfaha, F4/80+Ly6Chigh macrophages lead to cell plasticity and cancer initiation in colitis, *Gastroenterology* 164 (2023) 593–609.
- [3] T. Kobayashi, B. Siegmund, C. Le Berre, S.C. Wei, M. Ferrante, B. Shen, C. N. Bernstein, S. Danese, L. Peyrin-Biroulet, T. Hibi, Ulcerative colitis, *Nat. Rev. Dis. Prim.* 6 (2020) 74.
- [4] S. Singh, Positioning therapies for the management of inflammatory bowel disease, *Nat. Rev. Gastroenterol. Hepatol.* 20 (2023) 411–412.
- [5] T.L. Parigi, F. D'Amico, M.T. Abreu, A. Dignass, I. Dotan, F. Magro, A.M. Griffiths, V. Jairath, M. Iacucci, G.J. Mantzaris, C. O'Morain, W. Reinisch, D.B. Sachar, D. Turner, T. Yamamoto, D.T. Rubin, L. Peyrin-Biroulet, S. Ghosh, S. Danese, Difficult-to-treat inflammatory bowel disease: results from an international consensus meeting, *Lancet Gastroenterol. Hepatol.* 8 (2023) 853–859.
- [6] R.J. Xavier, D.K. Podolsky, Unravelling the pathogenesis of inflammatory bowel disease, *Nature* 448 (2007) 427–434.
- [7] F. Cao, L. Jin, Y. Gao, Y. Ding, H. Wen, Z. Qian, C. Zhang, L. Hong, H. Yang, J. Zhang, Z. Tong, W. Wang, X. Chen, Z. Mao, Artificial-enzymes-armed *Bifidobacterium longum* probiotics for alleviating intestinal inflammation and microbiota dysbiosis, *Nat. Nanotechnol.* 18 (2023) 617–627.
- [8] S. Liu, W. Zhao, P. Lan, X. Mou, The microbiome in inflammatory bowel diseases: from pathogenesis to therapy, *Protein Cell* 12 (2021) 331–345.
- [9] Q. Huang, Y. Yang, Y. Zhu, Q. Chen, T. Zhao, Z. Xiao, M. Wang, X. Song, Y. Jiang, Y. Yang, J. Zhang, Y. Xiao, Y. Nan, W. Wu, K. Ai, Oral metal-free melanin nanozymes for natural and durable targeted treatment of inflammatory bowel disease (IBD), *Small* 19 (2023) e2207350.
- [10] A.R. Bourgonje, M. Feilich, K.N. Faber, A. Pasch, G. Dijkstra, H. van Goor, Oxidative stress and redox-modulating therapeutics in inflammatory bowel disease, *Trends Mol. Med.* 26 (2020) 1034–1046.
- [11] E.L. Campbell, S.P. Colgan, Control and dysregulation of redox signalling in the gastrointestinal tract, *Nat. Rev. Gastroenterol. Hepatol.* 16 (2019) 106–120.
- [12] M. Schirmer, A. Garner, H. Vlamakis, R.J. Xavier, Microbial genes and pathways in inflammatory bowel disease, *Nat. Rev. Microbiol.* 17 (2019) 497–511.
- [13] W. Zhu, M.G. Winter, M.X. Byndloss, L. Spiga, B.A. Duerkop, E.R. Hughes, L. Buttner, E. de Lima Romao, C.L. Behrendt, C.A. Lopez, L. Sifuentes-Dominguez, K. Huff-Hardy, R.P. Wilson, C.C. Gillis, C. Tukul, A.Y. Koh, E. Burstein, L.V. Hooper, A.J. Baumler, S.E. Winter, Precision editing of the gut microbiota ameliorates colitis, *Nature* 553 (2018) 208–211.
- [14] A.C. Fenneman, M. Weidner, L.A. Chen, M. Nieuwdorp, M.J. Blaser, Antibiotics in the pathogenesis of diabetes and inflammatory diseases of the gastrointestinal tract, *Nat. Rev. Gastroenterol. Hepatol.* 20 (2023) 81–100.
- [15] L.H. Nguyen, A.K. Ortqvist, Y. Cao, T.G. Simon, B. Roelstraete, M. Song, A.D. Joshi, K. Staller, A.T. Chan, H. Khalili, O. Olen, J.F. Ludvigsson, Antibiotic use and the development of inflammatory bowel disease: a national case-control study in Sweden, *Lancet Gastroenterol. Hepatol.* 5 (2020) 986–995.
- [16] Y. Yu, X. Zhao, X. Xu, C. Cai, X. Tang, Q. Zhang, L. Zhong, F. Zhou, D. Yang, Z. Zhu, Rational design of orally administered cascade nanozyme for inflammatory bowel disease therapy, *Adv. Mater.* 35 (2023) e2304967.
- [17] J. Zhao, W. Gao, X. Cai, J. Xu, D. Zou, Z. Li, B. Hu, Y. Zheng, Nanozyme-mediated catalytic nanotherapy for inflammatory bowel disease, *Theranostics* 9 (2019) 2843–2855.
- [18] H. Yao, F. Wang, H. Chong, J. Wang, Y. Bai, M. Du, X. Yuan, X. Yang, M. Wu, Y. Li, H. Pang, A curcumin-modified coordination polymers with ROS scavenging and macrophage phenotype regulating properties for efficient ulcerative colitis treatment, *Adv. Sci.* 10 (2023) e2300601.
- [19] Y. Tian, Y. Li, J. Liu, Y. Lin, J. Jiao, B. Chen, W. Wang, S. Wu, C. Li, Photothermal therapy with regulated Nrf2/NF- κ B signaling pathway for treating bacteria-induced periodontitis, *Bioact. Mater.* 9 (2022) 428–445.
- [20] H. He, Q. Han, S. Wang, M. Long, M. Zhang, Y. Li, Y. Zhang, N. Gu, Design of a multifunctional nanozyme for resolving the proinflammatory plaque microenvironment and attenuating atherosclerosis, *ACS Nano* 17 (2023) 14555–14571.
- [21] M. Wang, Q. Huang, M. Liu, T. Zhao, X. Song, Q. Chen, Y. Yang, Y. Nan, Z. Liu, Y. Zhang, W. Wu, K. Ai, Precisely inhibiting excessive intestinal epithelial cell apoptosis to efficiently treat inflammatory bowel disease with oral pifithrin- α -embedded nanomedicine (OPEN), *Adv. Mater.* 35 (2023) e2309370.
- [22] J. Xu, J. Xu, T. Shi, Y. Zhang, F. Chen, C. Yang, X. Guo, G. Liu, D. Shao, K.W. Leong, G. Nie, Probiotic-inspired nanomedicine restores intestinal homeostasis in colitis by regulating redox balance, immune responses, and the gut microbiome, *Adv. Mater.* 35 (2023) e2207890.
- [23] M. Duran-Lobato, Z. Niu, M.J. Alonso, Oral delivery of biologics for precision medicine, *Adv. Mater.* 32 (2020) e1901935.
- [24] Z. Cao, S. Cheng, X. Wang, Y. Pang, J. Liu, Camouflaging bacteria by wrapping with cell membranes, *Nat. Commun.* 10 (2019) 3452.
- [25] X. Zhang, X. Xu, Y. Chen, Y. Dou, X. Zhou, L. Li, C. Li, H. An, H. Tao, H. Hu, X. Li, J. Zhang, Bioinspired yeast microcapsules loaded with self-assembled nanotherapies for targeted treatment of cardiovascular disease, *Mater. Today* 20 (2017) 301–313.
- [26] X. Zhang, Z. Yuan, J. Wu, Y. He, G. Lu, D. Zhang, Y. Zhao, R. Wu, Y. Lv, K. Cai, S. He, An orally-administered nanotherapeutics with carbon monoxide supplying for inflammatory bowel disease therapy by scavenging oxidative stress and restoring gut immune homeostasis, *ACS Nano* 17 (2023) 21116–21133.
- [27] S. Zhao, Y. Li, Q. Liu, S. Li, Y. Cheng, C. Cheng, Z. Sun, Y. Du, C.J. Butch, H. Wei, An orally administered CeO₂@Montmorillonite nanozyme targets inflammation for inflammatory bowel disease therapy, *Adv. Funct. Mater.* 30 (2020) 2004692.
- [28] Y. Peng, X. Luo, Z. Li, X. Fan, Y. Wang, R.R. He, M. Liu, A ferroporphyrin-anchored halloysite as orally drug delivery system for radiation colitis therapy, *Nat. Commun.* 14 (2023) 5083.
- [29] H. He, Q. Qin, F. Xu, Y. Chen, S. Rao, C. Wang, X. Jiang, X. Lu, C. Xie, Oral polyphenol-armed nanomedicine for targeted modulation of gut microbiota–brain interactions in colitis, *Sci. Adv.* 9 (2023) eadf3887.
- [30] H. Luo, Y. Chen, X. Kuang, X. Wang, F. Yang, Z. Cao, L. Wang, S. Lin, F. Wu, J. Liu, Chemical reaction-mediated covalent localization of bacteria, *Nat. Commun.* 13 (2022) 7808.
- [31] C.N. Spaulding, R.D. Klein, S. Ruer, A.L. Kau, H.L. Schreiber, Z.T. Cusumano, K. W. Dodson, J.S. Pinkner, D.H. Fremont, J.W. Janetka, H. Remaut, J.I. Gordon, S. J. Hultgren, Selective depletion of uropathogenic *E. coli* from the gut by a FimH antagonist, *Nature* 546 (2017) 528–532.
- [32] W. Zhang, L. Xu, H.-B. Park, J. Hwang, M. Kwak, P.C.W. Lee, G. Liang, X. Zhang, J. Xu, J.-O. Jin, *Escherichia coli* adhesion portion FimH functions as an adjuvant for cancer immunotherapy, *Nat. Commun.* 11 (2020) 1187.
- [33] A.M. Fleming, C.J. Burrows, On the irrelevancy of hydroxyl radical to DNA damage from oxidative stress and implications for epigenetics, *Chem. Soc. Rev.* 49 (2020) 6524–6528.
- [34] B. Yang, H. Yao, J. Yang, C. Chen, J. Shi, Construction of a two-dimensional artificial antioxidant for nanocatalytic rheumatoid arthritis treatment, *Nat. Commun.* 13 (2022) 1988.
- [35] W. Peng, X. Han, H. Hu, M. Chang, L. Ding, H. Xiang, Y. Chen, Y. Li, 2D vanadium carbide MXene to alleviate ROS-mediated inflammatory and neurodegenerative diseases, *Nat. Commun.* 12 (2021) 2203.
- [36] Y. Tian, W. Gui, I. Koo, P.B. Smith, E.L. Allman, R.G. Nichols, B. Rimal, J. Cai, Q. Liu, A.D. Patterson, The microbiome modulating activity of bile acids, *Gut Microb.* 11 (2020) 979–996.
- [37] P. Liu, P. Ji, L. Wang, H. Guo, M. Huo, J. Shi, Concurrent antibiosis and anti-inflammation against bacterial pneumonia by zinc hexacyanoferrate nanocatalysts, *Biomaterials* 289 (2022) 121768.
- [38] J. Zhang, M. Zhang, X.K. Huo, J. Ning, Z.L. Yu, C. Morisseau, C.P. Sun, B. D. Hammock, X.C. Ma, Macrophage inactivation by small molecule wedelolactone via targeting sEH for the treatment of LPS-induced acute lung injury, *ACS Cent. Sci.* 9 (2023) 440–456.
- [39] J.D. Lambeth, A.S. Neish, Nox enzymes and new thinking on reactive oxygen: a double-edged sword revisited, *Annu. Rev. Pathol.* 9 (2014) 119–145.
- [40] A. Lao, J. Wu, D. Li, A. Shen, Y. Li, Y. Zhuang, K. Lin, J. Wu, J. Liu, Functionalized metal-organic framework-modified hydrogel that breaks the vicious cycle of inflammation and ROS for repairing of diabetic bone defects, *Small* 19 (2023) e2206919.
- [41] C. Zhang, H. Wang, X. Yang, Z. Fu, X. Ji, Y. Shi, J. Zhong, W. Hu, Y. Ye, Z. Wang, D. Ni, Oral zero-valent-molybdenum nanodots for inflammatory bowel disease therapy, *Sci. Adv.* 8 (2022) eabp9882.
- [42] J. Yang, G. Zhang, M. Peng, S. Tan, S. Ge, X. Yang, Y. Liang, Z. Wen, L. Xie, T. Zhou, S. Wu, J. An, Y. Wang, W. Liu, K. Zhang, Z. Zhang, J. Liu, J. Shi, Bionic regulators break the ecological niche of pathogenic bacteria for modulating dysregulated microbiome in colitis, *Adv. Mater.* 34 (2022) e2204650.
- [43] S. Lin, S. Mukherjee, J. Li, W. Hou, C. Pan, J. Liu, Mucosal immunity-mediated modulation of the gut microbiome by oral delivery of probiotics into Peyer's patches, *Sci. Adv.* 7 (2021) eabf0677.
- [44] N. Zhao, F.-E. Yang, C.-Y. Zhao, S.-W. Lv, J. Wang, J.-M. Liu, S. Wang, Construction of pH-dependent nanozymes with oxygen vacancies as the high-efficient reactive oxygen species scavenger for oral-administrated anti-inflammatory therapy, *Adv. Healthc. Mater.* 10 (2021) e2101618.
- [45] S. Massironi, C. Viganò, A. Palermo, L. Pirola, G. Mulinacci, M. Allocca, L. Peyrin-Biroulet, S. Danese, Inflammation and malnutrition in inflammatory bowel disease, *Lancet Gastroenterol. Hepatol.* 8 (2023) 579–590.
- [46] D. Yoo, C.-H. Whang, J. Hong, D. Kim, M.C. Prayogo, Y. Son, W. Jung, S. Lee, H.-S. Lee, S. Jon, Anti-inflammatory glycoalkaloid-mimicking nanoparticles for colitis treatment: construction and in vivo evaluation, *Angew. Chem., Int. Ed.* 62 (2023) e202304815.
- [47] B. Wu, L. Qiang, Y. Zhang, Y. Fu, M. Zhao, Z. Lei, Z. Lu, Y.-G. Wei, H. Dai, Y. Ge, M. Liu, X. Zhou, Z. Peng, H. Li, C.-P. Cui, J. Wang, H. Zheng, C.H. Liu, L. Zhang, The deubiquitinase OTUD1 inhibits colonic inflammation by suppressing RIPK1-mediated NF- κ B signaling, *Cell. Mol. Immunol.* 19 (2022) 276–289.
- [48] M. Jarosz, M. Olbert, G. Wyszogrodzka, K. Mlyniec, T. Librowski, Antioxidant and anti-inflammatory effects of zinc. Zinc-dependent NF- κ B signaling, *Inflammopharmacology* 25 (2017) 11–24.
- [49] Y. Higashimura, T. Takagi, Y. Naito, K. Uchiyama, K. Mizushima, M. Tanaka, M. Hamaguchi, Y. Itoh, Zinc deficiency activates the IL-23/Th17 Axis to aggravate experimental colitis in mice, *J. Crohns Colitis* 14 (2020) 856–866.
- [50] S. Siva, D.T. Rubin, G. Gulotta, K. Wroblewski, J. Pekow, Zinc deficiency is associated with poor clinical outcomes in patients with inflammatory bowel disease, *Inflamm. Bowel Dis.* 23 (2017) 152–157.
- [51] Y. Wan, B. Zhang, The impact of zinc and zinc homeostasis on the intestinal mucosal barrier and intestinal diseases, *Biomolecules* 12 (2022) 900.
- [52] E.E.L. Nyström, B. Martínez-Abad, L. Arike, G.M.H. Birchenough, E.B. Nonnecke, P. A. Castillo, F. Svensson, C.L. Bevins, G.C. Hansson, M.E.V. Johansson, An intercrypt subpopulation of goblet cells is essential for colonic mucus barrier function, *Science* 372 (2021) eabb1590.
- [53] X.L. Hu, W. Xiao, Y. Lei, A. Green, X. Lee, M.R. Maradana, Y. Gao, X. Xie, R. Wang, G. Chennell, M.A. Basson, P. Kille, W. Maret, G.A. Bewick, Y. Zhou, C. Hogstrand,

- Aryl hydrocarbon receptor utilises cellular zinc signals to maintain the gut epithelial barrier, *Nat. Commun.* 14 (2023) 5431.
- [54] K.L. Glassner, B.P. Abraham, E.M.M. Quigley, The microbiome and inflammatory bowel disease, *J. Allergy Clin. Immunol.* 145 (2020) 16–27.
- [55] R. Caruso, B.C. Lo, G. Núñez, Host-microbiota interactions in inflammatory bowel disease, *Nat. Rev. Immunol.* 20 (2020) 411–426.
- [56] I. Lagkouvardos, T.R. Lesker, T.C.A. Hitch, E.J.C. Galvez, N. Smit, K. Neuhaus, J. Wang, J.F. Baines, B. Abt, B. Stecher, J. Overmann, T. Strowig, T. Clavel, Sequence and cultivation study of Muribaculaceae reveals novel species, host preference, and functional potential of this yet undescribed family, *Microbiome* 7 (2019) 28.
- [57] J. Schulthess, S. Pandey, M. Capitani, K.C. Rue-Albrecht, I. Arnold, F. Franchini, A. Chomka, N.E. Ilott, D.G.W. Johnston, E. Pires, J. McCullagh, S.N. Sansom, C. V. Arancibia-Carcamo, H.H. Uhlig, F. Powrie, The short chain fatty acid butyrate imprints an antimicrobial Program in macrophages, *Immunity* 50 (2019) 432–445 e7.
- [58] M.T. Sorbara, E.R. Littmann, E. Fontana, T.U. Moody, C.E. Kohout, M. Gjonbalaj, V. Eaton, R. Seok, I.M. Leiner, E.G. Pamer, Functional and genomic variation between human-derived isolates of Lachnospiraceae reveals inter- and intra-species diversity, *Cell Host Microbe* 28 (2020) 134–146.
- [59] A. Koh, F. De Vadder, P. Kovatcheva-Datchary, F. Backhed, From dietary fiber to host physiology: short-chain fatty acids as key bacterial metabolites, *Cell* 165 (2016) 1332–1345.
- [60] S.R. Sinha, Y. Haileselassie, L.P. Nguyen, C. Tropini, M. Wang, L.S. Becker, D. Sim, K. Jarr, E.T. Spear, G. Singh, H. Namkoong, K. Bittinger, M.A. Fischbach, J. L. Sonnenburg, A. Habtezion, Dysbiosis-induced secondary bile acid deficiency promotes intestinal inflammation, *Cell Host Microbe* 27 (2020) 659–670.
- [61] P.D. Cani, C. Depommier, M. Derrien, A. Everard, W.M. de Vos, Akkermansia muciniphila: paradigm for next-generation beneficial microorganisms, *Nat. Rev. Gastroenterol. Hepatol.* 19 (2022) 625–637.
- [62] E.L. Campbell, S.P. Colgan, Control and dysregulation of redox signalling in the gastrointestinal tract, *Nat. Rev. Gastroenterol. Hepatol.* 16 (2019) 106–120.
- [63] S.E. Winter, M.G. Winter, M.N. Xavier, P. Thiennimitr, V. Poon, A.M. Kestra, R. C. Laughlin, G. Gomez, J. Wu, S.D. Lawhon, I.E. Popova, S.J. Parikh, L.G. Adams, R.M. Tsolis, V.J. Stewart, A.J. Baumber, Host-derived nitrate boosts growth of *E. coli* in the inflamed gut, *Science* 339 (2013) 708–711.
- [64] H.C. Mirsepasi-Lauridsen, B.A. Vallance, K.A. Krogfelt, A.M. Petersen, *Escherichia coli* pathobionts associated with inflammatory bowel disease, *Clin. Microbiol. Rev.* 32 (2019) e00060-18.
- [65] F. Cuskin, E.C. Lowe, M.J. Temple, Y. Zhu, E. Cameron, N.A. Pudlo, N.T. Porter, K. Urs, A.J. Thompson, A. Cartmell, A. Rogowski, B.S. Hamilton, R. Chen, T. J. Tolbert, K. Piens, D. Bracke, W. Vervecken, Z. Hakki, G. Speciale, J.L. Munöz-Munöz, A. Day, M.J. Peña, R. McLean, M.D. Suits, A.B. Boraston, T. Atherly, C. J. Ziemer, S.J. Williams, G.J. Davies, D.W. Abbott, E.C. Martens, H.J. Gilbert, Human gut Bacteroidetes can utilize yeast mannan through a selfish mechanism, *Nature* 517 (2015) 165–169.
- [66] C. Zhao, J. Li, S. Wang, Z. Xu, X. Wang, X. Liu, L. Wang, X. Huang, Membranization of coacervates into artificial phagocytes with predation toward bacteria, *ACS Nano* 15 (2021) 10048–10057.